Model-Based Loads Observer Approach for Landing Gear Remaining Useful Life Prediction

Jonathan Jobmann[1] and Frank Thielecke[2]

[1,2] *Institute of Aircraft Systems Engineering – Hamburg University of Technology, Hamburg, 21129, Germany*
jonathan.jobmann@tuhh.de
frank.thielecke@tuhh.de

ABSTRACT

Implementing health monitoring methods for aircraft landing gears holds the potential to prevent premature component replacements and optimize maintenance scheduling. Therefore, this paper introduces a fundamental framework for fatigue monitoring and subsequent steps for predicting the remaining useful life of landing gears. A key component of this framework is the model-based load observer, which lays the groundwork for subsequent remaining useful life prediction steps. This load observer will be analysed in detail in this paper. The model-based approach is specifically designed for observing the loads on civil aircraft landing gears during touchdown, utilizing signals from in-service sensors. To evaluate the load observation method, a flexible multibody simulation model is introduced to generate synthetic data sets of aircraft in-service data and the corresponding landing gear loads, given the unavailability of real in-service and recorded landing gear load data. The load observation method is applied to synthetic in-service data across various virtually performed landing scenarios, offering a proof of concept along with extensive analysis of parameter uncertainties and additional factors influencing observation quality. Through this analysis, certain challenges to the observation method are identified that require further investigation in subsequent research efforts.

1. INTRODUCTION

Optimizing aircraft life cycle management significantly contributes to enhancing profitability and maintaining competitiveness within the aircraft industry, while also facilitating the achievement of ambitious climate objectives. One essential aspect of an aircraft's life cycle involves its operational life, including maintenance. Emerging maintenance strategies, such as condition-based, predictive, and prescriptive maintenance, prioritize health-oriented approaches aiming to optimize aircraft operating life by enhancing performance and safety. The advancement of processes and methodologies for these strategies is facilitated by the growing digitization and improved IT infrastructure, notably through digital platforms that address aircraft operational life and maintenance needs. This technological advancement enables the intensive computation and memory utilization required for certain health monitoring methods, which contribute to an optimized aircraft life cycle management. Especially structural components, such as aircraft landing gears (LG), offer high potential for the meaningful implementation of health monitoring methods.

LG systems must endure a variety of severe loads across different loading conditions. To ensure the structural integrity of the LG, with no detectable fatigue cracking throughout its operational lifespan, the safe life design philosophy is commonly employed in structural LG design (Schmidt, 2021). In this context, the safe life denotes the duration during which the components can operate without experiencing fatigue cracking. At the latest, when this point in time is reached or exceeded, the components are retired from service. Designing with the safe life philosophy entails incorporating scatter factors and estimating fatigue load spectra (SAE International, 2020), often resulting in underestimated individual LG lifespans.

However, by gaining detailed insights into actual loads and fatigue experienced during service, the assessment of LG condition and the prognosis of remaining useful life (RUL) can be performed. Consequently, implementing Structural Health Monitoring (SHM) for LGs through fatigue monitoring methods may help avoid premature replacements and optimize maintenance scheduling. Furthermore, the comprehensive understanding of the actual loads experienced in service opens up opportunities to improve future LG designs (Schmidt & Sartor, 2009).

In recent years, several fatigue monitoring approaches have been developed for aircraft, with some specifically tailored for LGs. One common feature among many of these aircraft fatigue monitoring approaches is the observation of loads prior to fatigue calculation. In (Boller & Buderath, 2007), (Boller & Staszewski, 2004), (Buderath & Neumair, 2007), (Buderath,

2009) and (Schmidt & Sartor, 2009) aircraft load observation approaches for fatigue monitoring are described.

One load monitoring approach involves using flight parameters monitored on the aircraft. Another SHM strategy utilizes additional sensors implemented on the aircraft, such as strain gauges. The data collected from these sensors can then be input into a ground-based digital loads model based on the finite element method. A similar approach, employing strain gauges, is addressed in (Chabod, 2022).

However, this approach incurs additional costs as it requires the installation of extra sensors on each LG to be monitored. Moreover, it increases the risk of sensor failures due to these additional sensors, which could affect aircraft availability or compromise the reliability of the implemented SHM methods. Conversely, employing model-based methods reliant on flight parameters extracted from sources like quick access recorder presents a promising strategy for observing LG loads and fatigue and can effectively mitigate these drawbacks. This approach is also already utilized for detecting transient overloads in LGs (Schmidt & Sartor, 2009).

Explicit research on fatigue monitoring of LGs primarily focuses on the utilization of machine learning methods. In (El Mir & Perinpanayagam, 2021), a machine learning model was proposed to determine load histories of the LG based on sensors onboard the aircraft. Additionally, (Holmes et al., 2016) presented results of a machine learning model calculating LG loads on different runway surfaces using sensor data collected from sensors attached to the LG. However, this approach has the disadvantage of requiring additional sensors to be installed on the LGs.

Addressing this limitation, (Jeong, Lee, Ham, Kim, & Cho, 2020) utilized a landing simulation model to generate synthetic flight parameters and related synthetic LG loads and strains for training machine learning models. Nonetheless, model-based methods offer several advantages over black box models like machine learning models. On the one hand, they are typically more robust and interpretable which is a great advantage within the certification process of aircraft systems. On the other hand, model-based approaches can be more efficient in using data, particularly in scenarios with limited data availability, as they often incorporate prior knowledge about the problem domain.

Therefore, this paper presents a model-based loads observer approach designed specifically for monitoring civil aircraft LG loads without the need for additional sensors, primarily utilizing in-service sensor signals as a foundational element. As the load observation of LG operations is very extensive and comes with various challenges, this paper aims to focus solely on the first landing impact of the main LGs. The developed method constitutes a key component of a comprehensive framework for fatigue monitoring in LGs. This framework, along with the steps for remaining useful life (RUL) prediction, is fundamentally introduced. The overall approach aims to lay the foundation for LG lifecycle management optimization through effective fatigue monitoring and prediction in future work.

The paper is organized as follows. The fatigue monitoring framework and subsequent steps for RUL calculation are introduced in Section 2. For detailed analysis of the model-based loads observer as a key component of the LG fatigue monitoring framework, Section 3 outlines the simulation model utilized for generating synthetic data. This synthetic data is essential for evaluating the loads observation method. Section 4 presents the description and analysis of this method. Finally, the paper concludes with Section 5, which provides a summary and a brief outlook.

2. FATIGUE MONITORING AND PREDICTION

In the following section the LG fatigue monitoring framework and an approach for downstream RUL prediction is presented.

2.1. Fatigue Monitoring Framework

There have been numerous publications addressing fatigue monitoring of aircraft structures, such as (Boller & Staszewski, 2004), (Buderath, 2009), (Dziendzikowski et al., 2021), (JIAO, HE, & LI, 2018), and (Stolz & Neumair, 2008). Additionally, publications by (El Mir & Perinpanayagam, 2021) and (El Mir & Perinpanayagam, 2022) have focused specifically on fatigue monitoring of LG systems. What most of these publications have in common is the proposed application of the Miner rule for calculating a health index of the structures. This rule calculates the cumulated damage D of structures over their life cycle using the equation

$$D = \sum \frac{n_i}{N_i}. \tag{1}$$

Applying n_i cycles with a certain stress amplitude i and the corresponding fatigue life endurance N_i on a structural component is equivalent to the consumption of n_i/N_i of fatigue resistance (Schijve, 2009). When the cumulated damage D reaches 1, failure is expected. Given that the Miner rule is presently utilized in the safe life fatigue analysis for LG certification processes (El Mir & Perinpanayagam, 2022), its application in the fatigue monitoring process of the LGs is evident. Therefore, the proposed fatigue monitoring framework in this paper also relies on the damage calculation using the Miner rule as a central element. By utilizing the Miner rule, many aspects of the fatigue monitoring framework are implicitly defined.

The LG fatigue monitoring framework, as illustrated in Figure 1, is based on the remaining life calculation scheme outlined in (Tinga, 2010) and the steps for safe-life analysis presented in (El Mir & Perinpanayagam, 2022). The objective of the

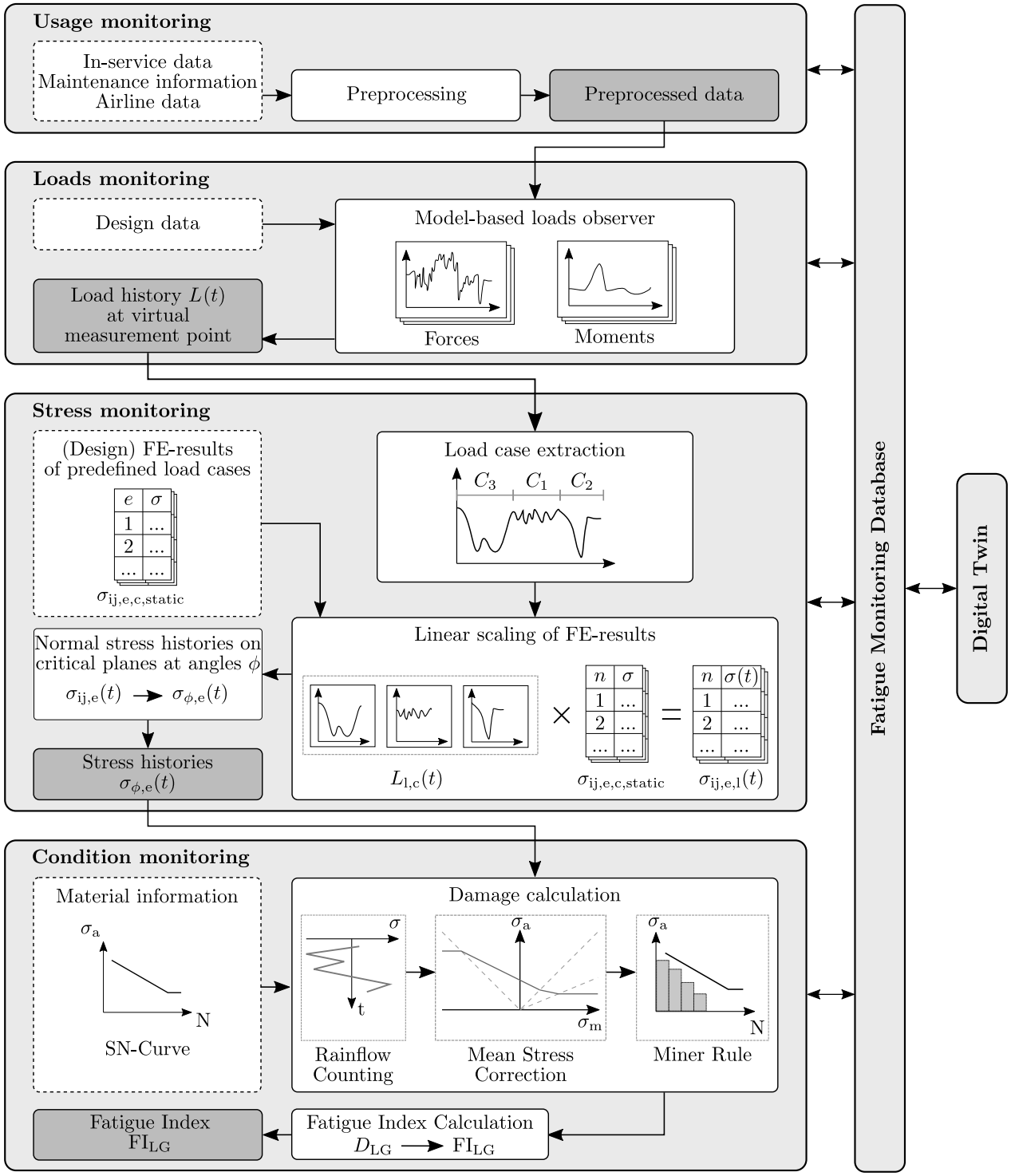

Figure 1. Schematic presentation of the LG fatigue monitoring framework

outlined framework is to present a comprehensive monitoring process for LGs, spanning from raw in-service data recordings over observing LG loads to monitoring LG fatigue and integrating digital twin technology. The framework serves as a basis for subsequent RUL calculation. Since real-time onboard aircraft fatigue monitoring is unnecessary and requires considerable storage and computing capacity, the framework operates offboard. Initially, usage monitoring is conducted within the framework, entailing the recording and storage of essential data, primarily in-service data. This data undergoes

preprocessing, including data cleansing and noise filtering. Subsequently, the preprocessed data is utilized to observe loads on the LG using simulation models constructed with LG design data, thereby virtually emulating the actual LG dynamics (model-based loads observer). The simulation model generates load histories at virtual load measurement points of the LG geometry. These specific locations are also used as load application points in finite element (FE) models for structural analysis. Thus, load histories and FE-models can be combined for subsequent stress monitoring.

To monitor LG structural stress based on LG load histories, stress tensors $\sigma_{\text{ij,e,c,static}}$ are calculated for selected 'hot spots' or across all finite elements e for different load cases c (e.g. specific steering, braking or landing conditions) using static FE design calculations, as depicted in Figure 1. The index ij represents the respective matrix entry of a stress tensor. To associate these stress tensors with observed loads, the load histories from the model-based loads observers are analysed, and specific load cases are extracted. The load histories are segmented into load events $L_{\text{l,c}}(t)$, where the additional index l denotes the index of the load event within the overall load history, and c links the load event to a specific FE load case. The stress tensors are then linearly scaled based on the load histories for each specific load event, resulting in a stress tensor history $\sigma_{\text{ij,e,l}}(t)$ for each finite element e and each load event l. This scaling is achieved through linear superposition by multiplying each load event with its corresponding stress tensor:

$$L_{\text{l,c}}(t) \cdot \sigma_{\text{ij,e,c,static}} = \sigma_{\text{ij,e,l}}(t). \tag{2}$$

It is important to note that each load event $L_{\text{l,c}}(t)$ is characterized by three force time series and three moment time series along the principal axes. However, the stress tensor is scaled by only one time series, which is selected based on the predominant force specific to the load case. Therefore, for each load event $L_{\text{l,c}}(t)$, the load case-specific predominant load is identified and used for scaling.

Afterwards, the stress tensor histories for all load events are chronologically ordered and concatenated for specific finite elements e, resulting in the combined stress tensor histories $\sigma_{\text{ij,e}}(t)$. To ensure accurate fatigue monitoring under complex, multiaxial loading conditions, the critical plane method is employed (Lee & Barkey, 2012). This method assesses stress across various potential planes to identify those where stresses and strains are most likely to cause damage. The stresses $\sigma_{\phi,\text{e}}$ on various planes of finite element e, oriented at angles ϕ under biaxial stress, are calculated using the formula:

$$\begin{aligned}\sigma_{\phi,\text{e}} =& \frac{\sigma_{\text{xx,e}} + \sigma_{\text{yy,e}}}{2} + \frac{\sigma_{\text{xx,e}} - \sigma_{\text{yy,e}}}{2} \cdot \cos 2\phi \\ &+ \tau_{xy,e} \cdot \sin 2\phi.\end{aligned} \tag{3}$$

Here, $\sigma_{\text{xx,e}}$ and $\sigma_{\text{yy,e}}$ represent the normal stresses on the x and y axes of the finite element, respectively, contributing both their average and their difference to the formula. Additionally, the formula includes the shear stress $\tau_{xy,e}$ across the plane. The output from the stress monitoring layer, as depicted in Figure 1, thus consists of the stress histories $\sigma_{\phi,\text{e}}$.

In order to apply the Miner rule, as stated in Equation 1, to the stress histories $\sigma_{\phi,\text{e}}$ within the condition monitoring layer depicted in Figure 1, the rainflow counting method is first performed. This method decomposes complex stress histories into a series of simple, reversed stress cycles, each representing an individual stress response that could potentially lead to material fatigue (Schijve, 2009). The output of the rainflow counting method includes the number of stress cycles n at specific stress amplitudes σ_{a} and mean stress levels σ_{m}. Additionally, the SN-Curve, schematically depicted in Figure 1, is crucial for applying the Miner rule (Schijve, 2009). This curve illustrates the relationship between stress amplitude σ_{a} (with mean stress level $\sigma_{\text{m}} = 0$) and the number of cycles to failure N for a given material. It is essential for implementing the Miner rule, which requires knowledge of the cycles to failure N for specific stress amplitudes. Each point on the SN-Curve represents a specific stress level and its corresponding fatigue life or life expectancy in terms of number of cycles.

Given that simple SN-Curves only address fatigue life under conditions of zero mean stress, mean stress correction is crucial for accurate fatigue life monitoring. The stress cycles n at specific stress amplitudes σ_{a} and mean stress levels σ_{m}, as determined by rainflow counting, are subject to mean stress correction, such as the Goodman mean stress correction method (Schijve, 2009). Once the stress amplitudes are corrected, the Miner rule, shown in Equation 1, can be applied. To assess the LG structural fatigue based on the stress histories $\sigma_{\phi,\text{e}}$ from the stress monitoring layer, the rainflow counting, mean stress correction, and Miner rule must be conducted for the stress histories on every plane at angle ϕ for each finite element e. Consequently, Equation 1 is extended to:

$$D_{\phi,\text{e}} = \sum \frac{n_{\phi,\text{e,i}}}{N_i}. \tag{4}$$

The maximum damage or fatigue D_{LG} experienced by the LG is calculated as follows:

$$D_{\text{LG}} = \max_{\phi,\text{e}} \left(D_{\phi,\text{e}} \right). \tag{5}$$

While calculating the maximum LG fatigue D_{LG} is critical, it is equally important to account for uncertainties in material performance and load observation, as outlined in (Schmidt, 2021). This consideration is implemented using a scatter factor (SF), which, for large civil aircraft, is a minimum of 3, corresponding to material properties with 99 % probability of survival and a 95 % confidence level, as specified by (European Union Aviation Safety Agency, 2020). Therefore,

the safe-life fatigue index $\mathrm{FI_{LG}}$ of the LG is calculated by:

$$\mathrm{FI_{LG}} = \mathrm{SF} \cdot D_{\mathrm{LG}}. \tag{6}$$

This health index serves as the health indicator within the condition monitoring layer of the framework.

The fatigue index, along with data from the usage, loads, stress, and condition monitoring blocks depicted in Figure 1, is stored in a fatigue monitoring database. This database ensures the availability and traceability of all information pertinent to the fatigue monitoring process. For enhanced traceability, it also includes additional information not shown in Figure 1, such as log cards detailing component removals. In conclusion, this database can be integrated into a digital twin or selectively transfer specific data to other systems.

2.2. Fatigue Prediction

The fatigue monitoring framework can be extended by incorporating a prognostics layer, as schematically depicted in Figure 2. Taking the fatigue index $\mathrm{FI_{LG}}$ as input, the RUL calculation

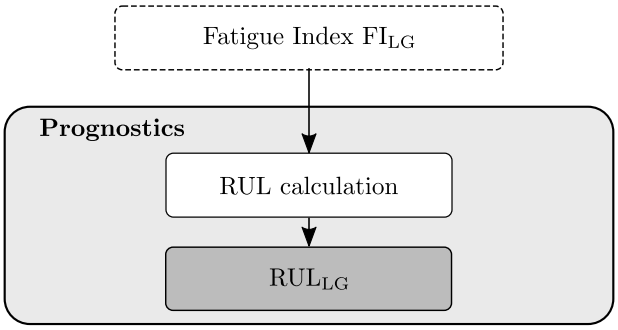

Figure 2. Schematic presentation of LG fatigue prognostics

is straightforward and requires only one main calculation step. Based on the remaining fatigue life estimations by (JIAO et al., 2018), the RUL of the LG is determined by

$$\mathrm{RUL_{LG}} = \frac{1 - \mathrm{FI_{LG}}}{\mathrm{SF} \cdot d} = \frac{1 - \mathrm{SF} \cdot D_{\mathrm{LG}}}{\mathrm{SF} \cdot d}, \tag{7}$$

where d is the predicted mean damage rate in subsequent service. If there is no difference in subsequent service expectable, then $d = 1$. The parameter $\mathrm{RUL_{LG}}$ indicates how much remaining life is left relative to 1, where a value of 1 corresponds to LG failure. To convert this RUL calculation into remaining flight cycles, the equation can be extended by the overall flight cycles n_{FC} experienced by the LG to predict the RUL in terms of remaining flight cycles $\mathrm{RUL_{LG,FC}}$:

$$\mathrm{RUL_{LG,FC}} = \frac{1 - \mathrm{SF} \cdot D_{\mathrm{LG}}}{\mathrm{SF} \cdot d} \cdot \frac{n_{\mathrm{FC}}}{D_{\mathrm{LG}}}. \tag{8}$$

Due to the various sources of uncertainties the precise determination of especially the scatter factor is demanding. The literature provides suggestions (Schmidt, 2021) but a probabilistic estimation of the scatter factor regarding the specific use should be performed when possible.

3. Base model for synthetic data generation

The development of monitoring methods typically requires some sort of data for evaluation. In this case, to assess the model-based LG loads observer, a combination of in-service data recorded by the quick access recorder and dedicated LG loads data is necessary. For this work, method development and evaluation should focus on a narrow-body airliner model with around 100-180 passengers serving as the reference aircraft.

However, due to the unavailability of in-service data and recorded dedicated LG loads, it is essential to generate plausible synthetic in-service and LG loads data. To achieve this, a base model was created using MATLAB/Simulink and the integrated library Simscape Multibody. Simscape Multibody facilitated the implementation of aircraft and LG components within a multibody simulation environment and provided seamless integration with Simulink.

The overall base model consists of the multibody LG model, the airframe, a runway and tyre model as well as an aircraft movement and control subsystem. Figure 3 provides a visualization of the basic model in Simscape Multibody. Further details regarding the structure of the base model are described in the subsequent section.

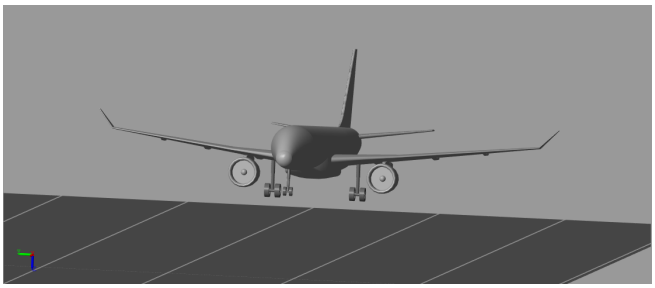

Figure 3. Visualization of the base model: multibody LG model, airframe and runway model

3.1. Multibody landing gear model

The implementation of the multibody LG model was based upon industrial design data, which was made available within the research project OBSERVATOR. Figure 4 illustrates the schematic representation of the implemented bodies and joints for a single main LG in the multibody model. The connection between the aircraft/airframe (AC) and the main fitting (MF) is modeled as a fixed joint (with no degrees of freedom) to represent the LG in an extended and locked state. Given that only load measurements at the LG wheel axle midpoint are of interest, as specified in Section 2.1 due to only one load

application point in the FE assembly model, no additional components connecting the LG and the aircraft, such as side stays, are modeled. However, the impact of these omitted components on LG flexibility is still addressed by integrating their flexibility into the overall LG flexibility matrices which are introduced later in this work.

For simulating translational shock absorber movement, a prismatic joint is installed between the MF and the sliding tube (ST), providing one translational degree of freedom. This design choice simplifies the multibody assembly, obviating the need for additional torque links to prevent ST rotation relative to MF along the rotational axis. Despite this design simplification, the loads calculation at the wheel axle midpoint is not affected. Moreover, to emulate LG flexibility, a single 6-DOF joint is utilized, condensing the LG flexibility into a single flexible point at the wheel axle midpoint. Additionally, revolute joints are employed to constrain the movement of LG wheels W1 and W2 to one rotational degree of freedom each.

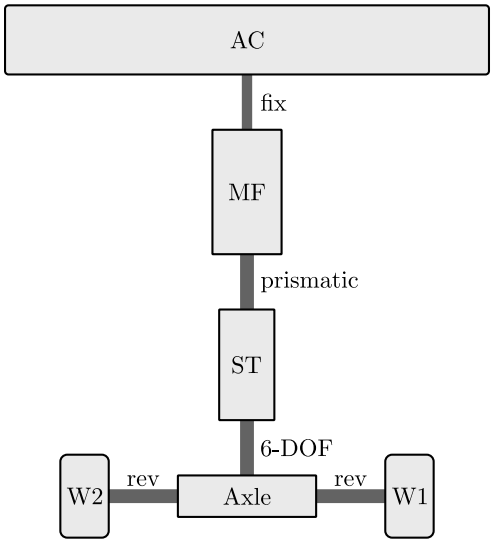

Figure 4. Schematic representation of the bodies and joints of a single main LG

One of the key components of the modeled nose LG configuration is the oleo-pneumatic shock absorber, which primarily provides spring suspension and damping of impact and recoil energy (Schmidt, 2021). To represent the vertical shock absorber dynamics, the shock absorber force, defined by

$$F_{\mathrm{SA}} = F_{\mathrm{spring}}\left(s_{\mathrm{SA}}, T_{\mathrm{amb}}\right) + F_{\mathrm{damp}}\left(s_{\mathrm{SA}}, \mathrm{sgn}(v_{\mathrm{SA}}), v_{\mathrm{SA}}^2\right) + F_{\mathrm{fric}} + F_{\mathrm{limit}}\left(s_{\mathrm{SA}}, v_{\mathrm{SA}}\right) \quad (9)$$

was implemented. Here, F_{spring} represents the force exerted by the gas spring, dependent on the shock absorber travel s_{SA} and ambient temperature T_{amb}. The term F_{damp} is a function of the shock absorber travel s_{SA}, shock absorber velocity $v_{\mathrm{SA}} = \dot{s}_{\mathrm{SA}}$, and the direction of velocity $\mathrm{sgn}(v_{\mathrm{SA}})$, reflecting the oil-induced damping force. Both, the gas spring and the damping force are modelled by the application of lookup tables. Additionally, the shock absorber force accounts for the friction force F_{fric} at the upper and lower bearings of the sliding tube by using simple friction coefficients, along with the translational limiting forces F_{limit} at the upper and lower stops of the shock absorber travel. These upper and lower limiting forces F_{limit} are modelled as simple spring-damper elements, dependent on s_{SA} and v_{SA}.

To implement a flexible LG model, the matrix equation of motion commonly employed in FE analysis was utilized in the LG model:

$$M\ddot{u} + C\dot{u} + Ku = F. \quad (10)$$

Here, F denotes the applied forces and the vector u represents the degrees of freedom of the FE model. M, C, and K denote the mass, damping, and stiffness matrices respectively. Due to computational complexity reduction reasons, only mass, damping and stiffness matrices of the order of 5 were available. With these system matrices reduced by the Guyan model order reduction method (GUYAN, 1965), the LG motion due to flexible structures could be simplified to only one point at the wheel axle midpoint. The computed LG motions were accurately replicated in the multibody model using the depicted 6-DOF joint in Figure 4. However, one translational degree of freedom along the shock absorber axis was disregarded due to the predominant shock absorber travel, leading to the utilization of only 5 degrees of freedom of the 6-DOF joint in Simscape Multibody.

What also had to be taken into account was the change in flexibility with varying shock absorber travel, so that Equation 10 changed to

$$M\left(s_{\mathrm{SA}}\right) \cdot \ddot{u} + C\left(s_{\mathrm{SA}}\right) \cdot \dot{u} + K\left(s_{\mathrm{SA}}\right) \cdot u = F. \quad (11)$$

This implementation issue was addressed by the usage of lookup tables as a function of the shock absorber travel in MATLAB/Simulink. The continuously calculated vector u of Equation 11 could then be input to the 6-DOF joint.

3.2. Tyre model

Tyres represent an essential component of vehicle dynamics such as aircraft LG dynamics. The forces and moments acting on the tyres during ground interaction greatly influence the vehicles dynamics. Thus, when developing multibody LG models, the tyre ground interaction has to be sufficiently represented by tyre models. In contrast to the multibody LG model, data for tyre modelling was not available. This proved to be a challenge, because tyre models in general rely on extensive input parameters. To address this issue, Fiala tyre models were chosen for modelling.The Fiala model is based on a brush-type tyre model and comes with the advantage, that it only requires 10 input parameters which are directly linked to physical properties of the tyre. Due to the fact, that Fiala tyre models for other aircraft types were available, the parameters of those

models could be used for parameter scaling so that plausible assumptions concerning the Fiala tyre models parameters could be made. Nevertheless, the usage of the Fiala model also comes with certain drawbacks as illustrated in (Blundell & Harty, 2004):

- Combined cornering and braking or cornering and accelerating is not considered in the model.
- Aligning moment and lateral force induced by the camber angle are not modelled.
- Varying cornering stiffness at zero slip angle with tyre load is not represented.
- At zero slip angle the offsets in lateral force or aligning moment due to conicity and ply steer are not considered.

Nevertheless, the Fiala tyre model represents a sufficiently good model for the usage of synthetic data generation for landing loads observation model evaluation. The exact mathematical representation of the model, which was used for implementation, is presented in (Blundell & Harty, 2004). The resulting forces and moments, calculated in MABLAB/Simulink, were used as inputs at the contact patches of the individual tyres in the multibody model.

3.3. Runway model

In order to simulate different tyre ground interactions for synthetic data generation, two different runways have been implemented in Simulink and visualized in Simscape Multibody:

- Even runway: A completely even runway with no bumps for optimal landing and taxiing conditions.
- San Francisco Runway 28R: The San Francisco Runway 28R before it was resurfaced was known for high loads on aircraft (European Union Aviation Safety Agency, 2020).

Both runway profiles were constructed using lookup tables in MATLAB/Simulink. The profile of San Francisco Runway 28R was developed based on specifications outlined in (European Union Aviation Safety Agency, 2020). Due to the lack of additional runway data, only these two profiles were employed for synthetic data generation. Within the simulation model, both runway profiles were linked with the tire models of each wheel to simulate tire-ground interaction. Figure 3 provides a visualization of a segment of the even runway.

3.4. Aircraft model and control

The aircraft, or airframe, was modelled as a single rigid body with specific mass and inertia properties. Since no information was available regarding the flight mechanics of similar-sized aircraft, aircraft movement was implemented using forces and moments primarily applied at the aircraft's center of gravity. By incorporating a six-degree-of-freedom joint at the aircraft's center of gravity, the aircraft could be maneuvered along all six degrees of freedom with the multibody LG model mounted on it. To simulate various landing scenarios, multiple controllers were developed. These controllers utilize the forces and moments acting on the aircraft as control variables, along with the aircraft's Euler angles and approach speeds in horizontal, lateral, and vertical directions as reference signals.

3.5. Synthetic data generation for different landing scenarios

The aim of this work, as mentioned in Section 1, is to present a method and evaluate it for observing landing loads in the context of LG fatigue monitoring and RUL prediction. Consequently, the generation of in-service data for various landing scenarios and the recording of dedicated LG loads were required. Simulated landing scenarios included level landings, one-gear landings, side load landings, and rebound landings. To create diverse landing conditions, different parameters were varied. These varied simulation parameters and their value ranges are outlined in Table 1. The variation limits represent plausible assumptions, partly based on knowledge of these parameters from similar aircraft or regulatory documents such as (European Union Aviation Safety Agency, 2020). For the variation of sensor sample rates, only rates up to 50 Hz are theoretically necessary, as higher sample rates are uncommon for aircraft quick access recorder data in today's commercial aviation industry. Nevertheless, additional in-service data sets with a sample rate of 200 Hz were recorded to assess the impact of higher sensor sample rates on monitoring performance.

Table 1. Overview of simulation parameter variations for synthetic data generation

Simulation parameter	**Variation limits**
Roll angle	± 5 deg
Pitch angle	$3 - 9$ deg
Yaw angle	± 5 deg
Aircraft mass	$50,000 - 60,000$ kg
Center of gravity	$22 - 28$ % MAC
Ground speed	$55 - 65$ m/s
Sinking speed	$0.3 - 3$ m/s
Sample rate (in-service data)	$20/50/200$ Hz
Measurement noise (in-service data)	no noise / white noise
Lift force	$0 - 1g$ (variable during touchdown)
Runway profile	even / San Francisco Runway 28R

4. Model-Based Loads Observation of Landing Gear Loads

The following section describes the model-based loads observer of LG loads at the initial landing impact. At first, the developed method is described. In a second step, results of the loads observation method are analysed and the method is evaluated.

4.1. Methodology

Aircraft model-based load observer approaches often rely on a Luenberger observer using specific system sensor data for state estimation, as demonstrated in (Montel & Thielecke, 2018) or (Luderer & Thielecke, 2022). Typically, in-service data recorded at the LG is limited to weight-on-wheel binary signals and rotational wheel speeds. However, employing state estimation within a Luenberger observer with feedback solely based on the the mentioned signals as the only LG signals is not feasible. Therefore, direct estimation of the LG dynamics and loads without state estimation feedback is utilized. A schematic representation of this method using a block diagram and a flow chart is depicted in Figure 5.

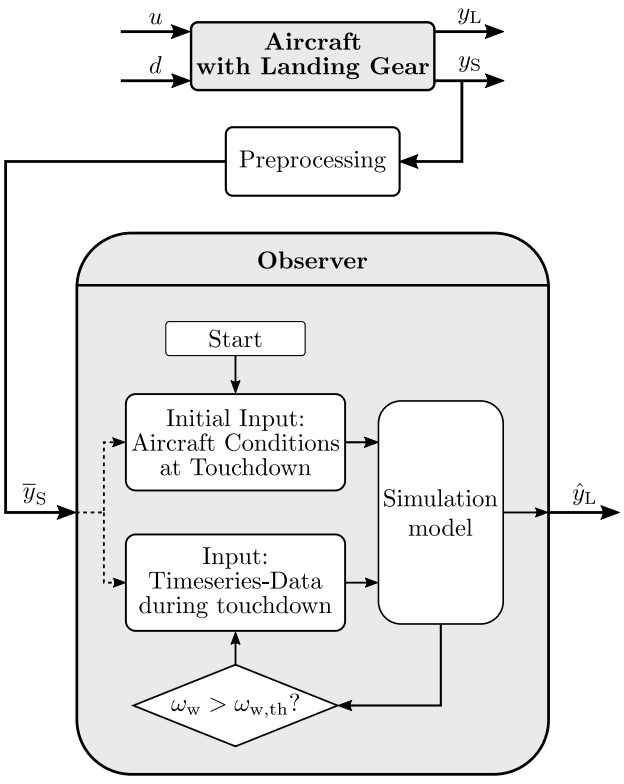

Figure 5. Block diagram of loads observer with data flow of schematic observer logic

During the landing phase and ground operations, the aircraft with the extended and locked LG is controlled with the aircraft inputs u and is simultaneously exposed to various external disturbances d. This results in various loads acting on the aircraft, and particularly in this work, loads y_L acting on the LG. The aircraft and LG dynamics are recorded by various sensors. The recorded in-service data y_S is preprocessed, as described in Section 2.1, so that the preprocessed data $\overline{y}_S$ can be used as loads observer input. The actual loads observer then tries to re-simulate the exact aircraft motion in an offboard simulation from the moment the rotational wheel speed ω_w of at least one main LG wheel exceeds the specified rotational wheel speed threshold $\omega_{w,th}$.

The loads observer begins simulating aircraft movement just above the runway. Initial inputs include the aircraft's roll and pitch angles and approach speeds recorded when the weight-on-wheel signal first changes to 'true' during touchdown. The observer simulates until the simulated rotational wheel speed ω_w of at least one main LG wheel exceeds the specified threshold $\omega_{w,th}$. After this point, the observer uses recorded time series data of longitudinal, vertical, and normal accelerations, roll, pitch, and yaw rates, as well as roll, pitch, and heading angles to reproduce the aircraft movement. The simulated loads are then output by the observer as the signal $\hat{y}_L$, as depicted in Figure 5.

4.2. Analysis

To assess the effectiveness of the proposed observer methodology, it was applied to various synthetic in-service data sets generated by the base model introduced in Section 3, with simulation parameters varied as detailed in Table 1. Initially, baseline simulations were conducted at a sample rate of 200 Hz on an even runway without measurement noise. This setup aimed to exclude potential influences such as uneven runways and low sensor sample rates, allowing for an analysis of the method's performance under 'ideal' conditions. Subsequently, the observer method was tested under more realistic conditions, including measurement noise, uneven runways, and sample rates of 20 Hz and 50 Hz.

A modified version of the base model was used as the simulation model for the model-based loads observer. After baseline and observer simulations, the simulated forces and moments at the main LG wheel axle midpoint during the initial load impact were compared. All observer simulations yielded highly accurate results, with deviations between the simulated baseline and observer loads being less than 2 %. Figure 6 illustrates the forces F_x and F_z at the wheel axle midpoint for a level landing scenario. Here, F_x denotes the force in the longitudinal direction, while F_z indicates the force in the vertical direction of the LG body-fixed coordinate system. The results show that the method performs well for various landing scenarios under conditions of no parameter uncertainties, no measurement noise, an even runway, and high sensor sample rates of 200 Hz or greater.

Subsequently, various parameters of the observer model were individually modified with plausible assumptions to account

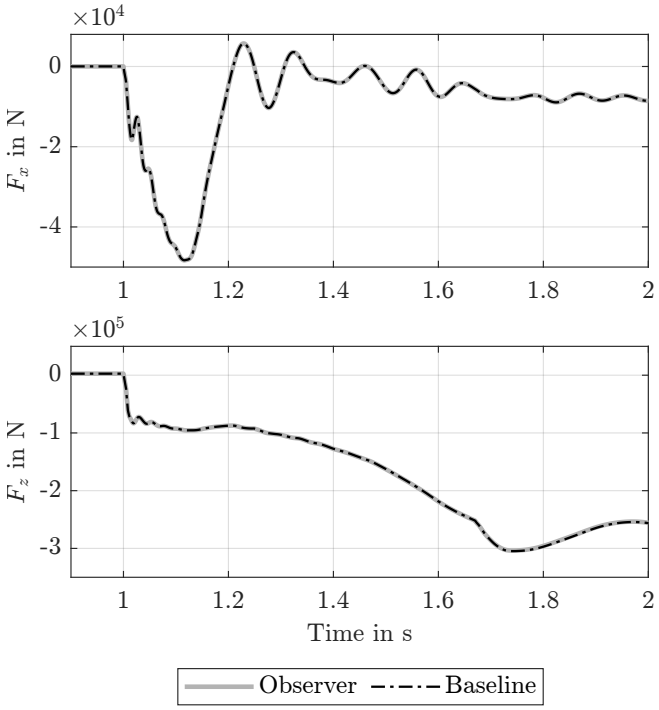

Figure 6. Load observation of longitudinal and vertical forces at wheel axle midpoint of one main LG at touchdown

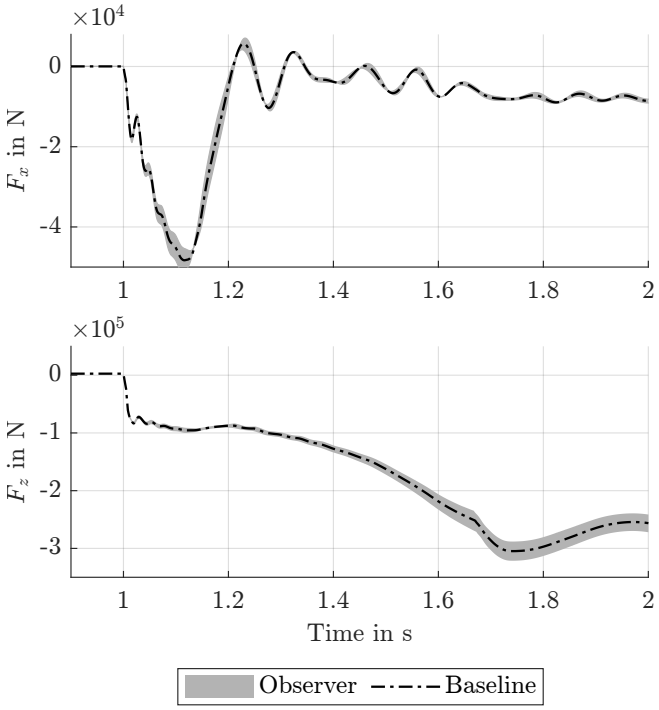

Figure 7. Load observation of longitudinal and vertical forces at wheel axle midpoint of one main LG at touchdown with shock absorber temperature uncertainty of $\pm 10°$ C at $30°$ C

for observer model uncertainties. The simulations were also conducted with high sample rates of 200 Hz and even runways to avoid biases in the analysis of model uncertainties. The varied parameters include LG flexibility matrices, shock absorber temperature uncertainty, shock absorber spring lookup table, shock absorber damping lookup table, sensor signal offsets, sensor positions, tyre friction coefficients, and tyre stiffness and damping coefficients. Despite these model uncertainties, the deviations between the baseline LG loads and the observer LG loads for the initial landing impact were less than 10 % and were therefore deemed sufficient. For example, Figure 7 illustrates the load estimation bandwidth of the observer for $\pm 10°$ C at $30°$ C shock absorber temperature uncertainty.

At the time of writing, the impact of the deviations between baseline and observer loads in the fatigue monitoring framework introduced in Section 2.1 is not fully known. Therefore, it is not yet possible to make exact statements about the quality of the observer results. Nonetheless, the initial findings indicate a potential for precise load monitoring despite model uncertainties.

Furthermore, the influence of sensor sample rates on the observer method has been examined. For example, the load observations of the longitudinal and vertical forces at the wheel axle midpoint are depicted for different sensor sample rates in Figure 8. While the observer performs well for load observation with sensor sample rates of 200 Hz, the quality of load estimation decreases with decreasing sample rate.

Figure 8 also reveals that both the observer with 20 Hz sample rate and the one with 50 Hz sample rate start to diverge from the baseline in F_z at approximately the same time. This occurrence can be attributed to a significant increase in the vertical deceleration of the aircraft about the same time, leading to imprecise recordings of vertical accelerations during observer simulations. Nevertheless, sample rates of 50 Hz, which are common in modern aircraft, still hold considerable potential for effective observation of LG loads during the initial landing impact at the main LGs for use in LG fatigue monitoring.

Another significant factor expected to influence load observation was landing on uneven runways. Baseline simulation results are depicted in Figure 9. These show the exemplary longitudinal and vertical forces at the wheel axle midpoint for a level landing scenario on the San Francisco Runway 28R profile (before resurfacing). This runway was known for inducing high loads due to its uneven nature. The figure also presents the corresponding observer loads simulated for an even runway, as the observer lacked information about the actual runway profile. An observer sample rate of 200 Hz was employed to mitigate potential inaccuracies from inadequate sample rates, thus excluding certain erroneous load estimations. At the beginning of the landing impact, when aircraft movement predominates and no critical runway bumps affect the LG, the observer estimates the LG loads quite accurately, albeit with higher frequency oscillations. However, as simulation time progresses, the loads begin to deviate significantly

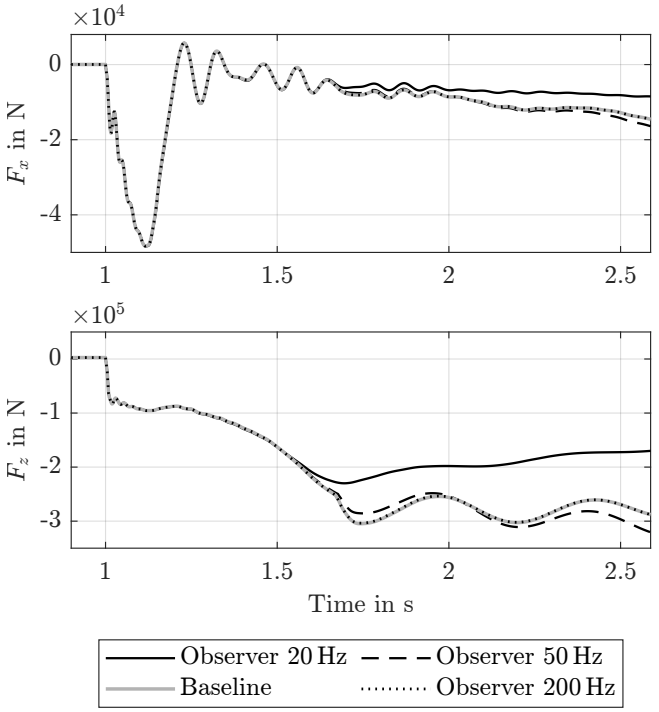

Figure 8. Loads observation of longitudinal and vertical forces at wheel axle midpoint of one main LG at touchdown for different virtual in-service data sample rates

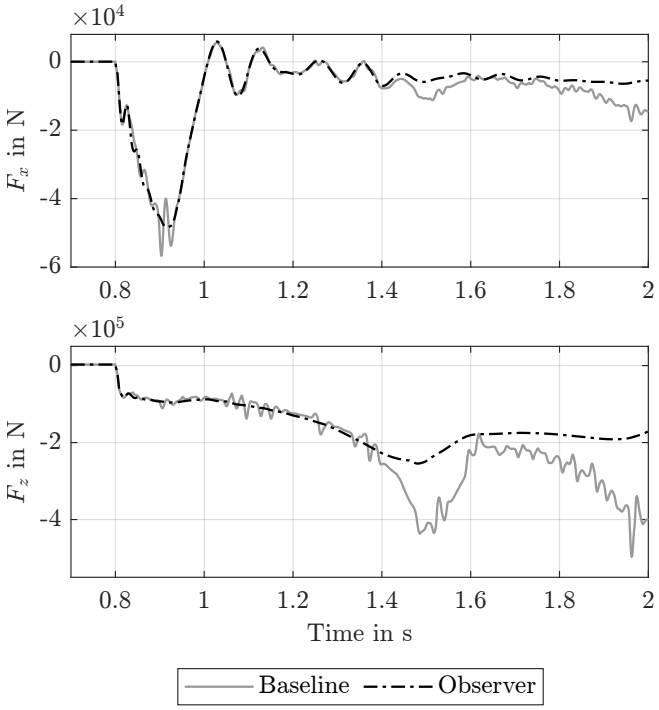

Figure 9. Loads observation of longitudinal and vertical forces at wheel axle midpoint of one main LG at touchdown: baseline touchdown on San Francisco Runway 28R profile, observer touchdown on even runway

due to runway bumps and variations in runway height.

The estimation results of the observer could be significantly improved by observer simulations with a known uneven runway profile and a known runway position of the aircraft during touchdown. However, if the precise landing position and especially the runway surface profile are unknown, which is usually the case nowadays, highly uneven runways can lead to significant variations in runway excitation. Despite maintaining the same vertical aircraft position in the observer as in the baseline, deviations in loads can be substantial due to these discrepancies.

5. Conclusion

This paper introduces a model-based LG loads observer method that operates exclusively on in-service data, thereby eliminating the need for additional sensors. The method is specifically evaluated with an emphasis on the first landing impact of the main LGs. It forms a key component of a comprehensive LG fatigue monitoring framework and the subsequent calculation of RUL for the LG. This paper also fundamentally outlines the foundational steps and further key components for LG fatigue monitoring and prediction, based on the 'safe life' design methodology commonly used for structural LG certification.

The application of the loads observer method on virtual in-service data with dedicated LG loads shows significant potential despite challenges, such as the unsuitability of LG feedback signals for state feedback observers and the heavy influence of sample rates on precision. For accurate load estimation, particularly for initial landing impacts, sample rates of at least 50 Hz are necessary. However, deviations between recorded and actual aircraft accelerations can lead to unacceptable estimation errors over time, suggesting that higher sample rates might be needed for longer monitoring durations.

A major challenge is the unknown runway profile, notably on uneven runways like the pre-resurfaced San Francisco Runway 28R, where load estimation accuracy drops significantly. The position inaccuracies in the observer model, due to integrating recorded aircraft accelerations, further distort load estimations on inclining runways. Precise runway profiles and exact touchdown coordinates are crucial for improving estimation accuracy.

While this paper demonstrates a basic proof of concept by applying the developed method to virtual in-service data, further analysis and development are required to address the challenges associated with load estimation. For instance, the exact effects of load estimation errors on fatigue and RUL determination need to be investigated. Additionally, knowledge about runway profiles and the exact touchdown position must be incorporated. Furthermore, combined effects of model uncertainties on load observation should be explored.

ACKNOWLEDGMENT

This work was funded by the German Federal Ministry for Economic Affairs and Climate Action within the project OBSERVATOR (contract code: 20D1903C) in the national LuFo program. Their support is greatly appreciated.

REFERENCES

Blundell, M., & Harty, D. (2004). *Multibody systems approach to vehicle dynamics*. Amsterdam: Elsevier Butterworth-Heinemann.

Boller, C., & Buderath, M. (2007). Fatigue in aerostructures — where structural health monitoring can contribute to a complex subject. *Philosophical Transactions of the Royal Society A: Mathematical, Physical and Engineering Sciences*, *365*(1851), 561–587. doi: 10.1098/rsta.2006.1924

Boller, C., & Staszewski, W. J. (2004). Aicraft structural health and usage monitoring. In W. J. Staszewski, C. Boller, & G. R. Tomlinson (Eds.), *Health monitoring of aerospace structures.* Chichester: John Wiley.

Buderath, M. (2009). Fatigue monitoring in military fixed-wing aircraft. In C. Boller, F.-K. Chang, & Y. Fujino (Eds.), *Encyclopedia of structural health monitoring.* Chichester: Wiley.

Buderath, M., & Neumair, M. (2007). Operational risk assessment for unmanned aircraft vehicles by using structural health and event management. *UAV Design Processes / Design Criteria for Structures*, 2.1-1 – 2.1-10.

Chabod, A. (2022). Digital twin for fatigue analysis. *Procedia Structural Integrity*, *38*, 382–392. doi: 10.1016/j.prostr.2022.03.039

Dziendzikowski, M., Kurnyta, A., Reymer, P., Kurdelski, M., Klysz, S., Leski, A., & Dragan, K. (2021). Application of operational load monitoring system for fatigue estimation of main landing gear attachment frame of an aircraft. *Materials (Basel, Switzerland)*, *14*(21). doi: 10.3390/ma14216564

El Mir, H., & Perinpanayagam, S. (2021). Certification approach for physics informed machine learning and its application in landing gear life assessment. In *2021 ieee/aiaa 40th digital avionics systems conference (dasc)* (pp. 1–6). IEEE. doi: 10.1109/DASC52595.2021.9594374

El Mir, H., & Perinpanayagam, S. (2022). Certification of machine learning algorithms for safe-life assessment of landing gear. *Frontiers in Astronomy and Space Sciences*, *9*. doi: 10.3389/fspas.2022.896877

European Union Aviation Safety Agency. (2020). Certification specifications and acceptable means of compliance for large aeroplanes cs-25: Amendment 26.

GUYAN, R. J. (1965). Reduction of stiffness and mass matrices. *AIAA Journal*, *3*(2), 380. doi: 10.2514/3.2874

Holmes, G., Sartor, P., Reed, S., Southern, P., Worden, K., & Cross, E. (2016). Prediction of landing gear loads using machine learning techniques. *Structural Health Monitoring*, *15*(5), 568–582. doi: 10.1177/1475921716651809

Jeong, S. H., Lee, K. B., Ham, J. H., Kim, J. H., & Cho, J. Y. (2020). Estimation of maximum strains and loads in aircraft landing using artificial neural network. *International Journal of Aeronautical and Space Sciences*, *21*(1), 117–132. doi: 10.1007/s42405-019-00204-2

JIAO, R., HE, X., & LI, Y. (2018). Individual aircraft life monitoring: An engineering approach for fatigue damage evaluation. *Chinese Journal of Aeronautics*, *31*(4), 727–739. doi: 10.1016/j.cja.2018.02.002

Lee, Y.-L., & Barkey, M. E. (2012). Stress-based multiaxial fatigue analysis. In Y.-L. Lee, M. E. Barkey, & H.-T. Kang (Eds.), *Metal fatigue analysis handbook.* Waltham, Mass: Butterworth-Heinemann.

Luderer, O., & Thielecke, F. (2022). Validation of a hybrid loads observer for a subscale test aircraft with distributed electric propulsion. *33rd Congress of the International Council of the Aeronautical Sciences ICAS*.

Montel, M., & Thielecke, F. (2018). Validation of a hybrid observer method for flight loads estimation. *31st Congress of the International Council of the Aeronautical Sciences, ICAS 2018*.

SAE International. (2020). *Landing gear fatigue spectrum development for part 25 aircraft: Air 5914.* 400 Commonwealth Drive, Warrendale, PA, United States: Author. doi: 10.4271/AIR5914

Schijve, J. (2009). *Fatigue of structures and materials* (Second edition ed.). Dordrecht: Springer.

Schmidt, R. K. (2021). *The design of aircraft landing gear*. SAE International. doi: 10.4271/9780768099430

Schmidt, R. K., & Sartor, P. (2009). Landing gear. In C. Boller, F.-K. Chang, & Y. Fujino (Eds.), *Encyclopedia of structural health monitoring.* Chichester: Wiley.

Stolz, C., & Neumair, M. (2008). Structural integrity management system for enhanced aircraft availability. *Future Airframe Structural Lifing: Methods, Applications and Management*, 24-1 - 24-12.

Tinga, T. (2010). Application of physical failure models to enable usage and load based maintenance. *Reliability Engineering & System Safety*, *95*(10), 1061–1075. doi: 10.1016/j.ress.2010.04.015